Supporting Information

A tri-modal paper device based on flower-like CuSe for the detection of Alzheimer Disease-associated microRNA marker

Yaqi Zhu, Yang Tian, and Tingting Zheng*

Shanghai Key Laboratory of Green Chemistry and Chemical Processes, Department of Chemistry, School of Chemistry and Molecular Engineering, East China Normal University, Dongchuan Road 500, Shanghai 200241, P. R. China

*E-mail: ttzheng@chem.ecnu.edu.cn

Table of Contents

S1. Experimental Sections

1.Chemicals and Reagents.

All of the chemicals were used without further purification and all aqueous solutions were prepared with Milli-Q water (18.2 MΩ·cm, Millipore). NaOH, CuCl, $FeCl_2$,KCl, NaCl, $ZnCl_2$, $CaCl_3$, and PVP (MW= 100000) were obtained from Sinopharm Chemical Reagent Co. Ltd (Shanghai, China). Se powder and 2,2'-Azino-Bis(3-Ethylbenzothiazoline-6-Sulfonic Acid) diammonium Salt (ABTS) were obtained from Sigma-Aldrich. Blood cell separation membrane (MF1), was purchased from Whatman (17 mm × 50 m) for the blood separation unit.

The microRNA sequences were obtained from Takara Biotechnology Co. Ltd. (Dalian, China), The DNA sequences were purchased from Shanghai Sangon Biological Engineering Technology & Services Co. (Shanghai, China). All the sequences were as follows:

miR-34c:5'-AGG CAG UGU AGU UAG CUG AUU GC-3'

Capture DNA : 5'-COOH-CCC CCC CCC CCC GCA ATC -3'

Detector DNA : 5'-AGC TAA CTA CAC TGC CTA AAA AAA AAA AA -SH-3'

RNA1: 5'-AGU CAG UGU AGU UAG CUG AUU GC-3'

RNA2: 5'-AGG CAG UGU AGU UAG CUG AUU AC-3'

RNA3: 5'-AGG CAG UGU AGU UAG CUG AUU AU-3'

RNA4: 5'-GCG CAG UGU AGU UAG CUG AUU GC-3'

RNA5: 5'-GGG GTA GCT TAT CAG ACT G-3'

miR-34a: 5'-UGG CAG UGU CUU AGC UGG UUG U-3'

miR-34b:5'-CAA UCA CUA ACU CCA CUG CCA U-3'

Mice in the early, middle and stage of AD and normal C57 mice were purchased from Shanghai Model Organisms.

2. Preparation of CuSe-modified DNA Probes.

1.5 mmol of CuCl and 100 mg of PVP (MW= 100 000) were added into 12.5 mL deionized water and stirred for 30 min. After that, 2.25 mmol of Se powder was added into the above solution and stirred for 30 min to form a uniform solution. It was then heated at 120°C for 2h in a Teflon-lined stainless-steel autoclave, followed by cooling naturally to room temperature. The product was centrifuged at 6000 rpm for 15 min and washed for several times. Finally, it was dried in vacuum at 70°C. Then, 3 μL of 100 μM thiolated DNA probes and 6 μL of 100 μM TCEP aqueous solution were mixed, and incubated at 25°C for 30 min. Then 1 mL CuSe (1.2 nM, pH=7.4) was added and incubated overnight. The product was separated by centrifugation at 10000 rpm for 30 min and rinsed with PBS (pH=7.4) for three times. The product was then dispersed in PBS buffer (10 mM, pH 7.4, 150 mM NaCl, 0.1% SDS) and stored at 4 °C.

3. Fabrication of paper device and miR-34c biosensing.

The device comprised detection unit, blood cell separation unit and a PDMS substrate. The blood cell separation unit was placed on the PDMS substrate and there was no additional combination between PDMS layer and separation unit. PDMS layer provided a hydrophobic surface, which prevented uncontrolled diffusion of plasma in device, ensuring the migration of plasma from drop site along the separation unit directly. The detection unit was modified with captured DNA. Briefly, 10μL 5% (3-Aminopropyl) trimethoxy-silane (APTMS) solution was added to the paper and incubated at room temperature for 30 min. After that, 5 μL 1 mM captured DNA was placed on the APTMS-modified paper and incubated for 30 minutes at 37°C in the presence of EDC and NHS. Then, 10 μL different concentrations of miR-34c was added into the device

and incubated for 30 min at 37°C. After that, 10 µL of the CuSe-modified DNA probes was added into the device and incubated for 30 min at 37 °C, forming the final detection unit for further analysis. Washing steps were carried out after each incubation step to remove non-specific binding. We used an incubator for temperature control to achieve the incubation temperature of 37°C. After hybridization, the solution containing ABTS (0.25 mg/mL), H_2O_2 (1.25 M) in 20 µL acetate buffer (0.1M, pH=4.2) was dropped on the device. After 15 min, qualitative results were obtained by observing the color changes from white to dark green. The UV-Vis absorption spectra of detection unit were collected by UV-vis spectrophotometer (UH5700, Hitachi, 220V). Meanwhile, the 808 nm laser (FU808AD1200-GD22, FU LASER) was used to irradiate each paper device for 2 min with a power density of 0.16 W/mm^2. The temperature was collected using a thermometer (MS32, ECOFIVE), which has a resolution of 0.1 °C and measuring range from -32°C to 390°C, immediately after irradiation. For Raman measurement, each paper device after incubation with ABTS and H_2O_2 was transferred to handheld Raman spectrometer (QE65 Pro, Ocean Optics, 220V) under 633 nm laser irradiation with exposure time of 1s. All experiments were carried out at room temperature (25°C).

4. Biosensing of miR-34c in whole blood using the developed paper device.

After anesthesia of the mice, blood was collected from mice following tail incision. All animal experiments were performed according to the guidelines of the Care and Use of Laboratory Animals formulated by the Ministry of Science and Technology of China and were approved by the Animal Care and Use Committee of East China Normal University. 20 µL whole blood was injected into the separation unit. After reaching the end of the separation unit, the captured DNA modified detection unit was placed at the end of separation units and contacted for 5 s in order to transfer the plasma to the detection unit. Then, remove the detection unit for the following measurement. Before the test, APTMS paper decorated with capture DNA probe as well as CuSe-modified detector DNA probe can be prepared in advance and stored at 4 °C for recent use and -20 °C for long-term storage, respectively. The CuSe-modified DNA probes were added and prehybridized for 30 min at 37 °C. After hybridization, the solution containing ABTS (0.25 mg/mL), H_2O_2 (1.25 M) in 20 µL acetate buffer (0.1M, pH=4.2) was dropped on the device. After 15 min, qualitative results were obtained by observing the color changes from white to dark green. The quantitative results were collected by UV-Vis-NIR absorption spectrometer, thermometer and handheld Raman spectroscopy, identical to those used in the previous miR-34c biosensing steps. All experiments were carried out at room temperature (25°C).

S2. Additional Figures

1. Scanning electron microscopic (SEM) image of flower-like CuSe.

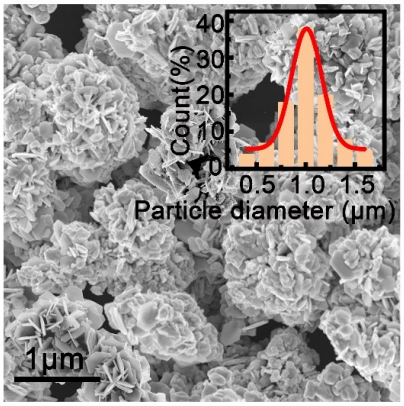

Fig. S1. SEM image of flower-like CuSe. Inset: size-distribution histograms of flower-like CuSe.

2. SEM and Energy-dispersive X-ray spectra (EDS) mapping image of CuSe nanoflake.

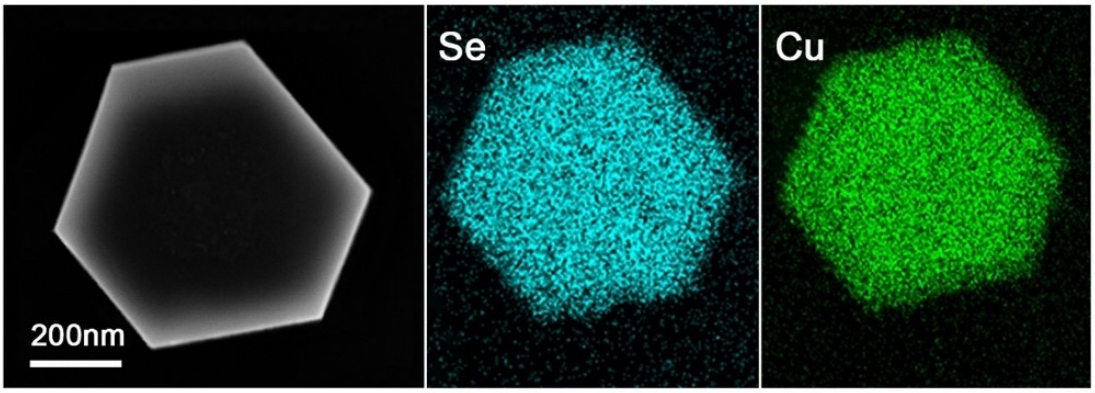

Fig. S2. The scanning electron microscopic (SEM) and Energy-dispersive X-ray spectra (EDS) mapping image of single CuSe nanoflake. The edge length of nanoflakes was 250 ± 50 nm (n=100).

3. X-ray diffraction (XRD) pattern of flower-like CuSe.

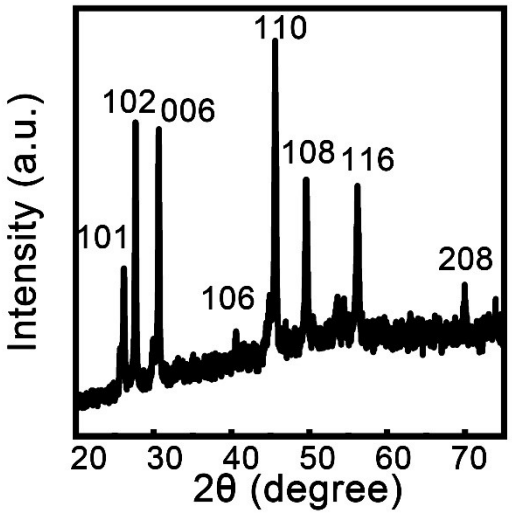

Fig. S3. XRD pattern of flower-like CuSe.

4. UV-Vis absorption spectra of CuSe nanoflake.

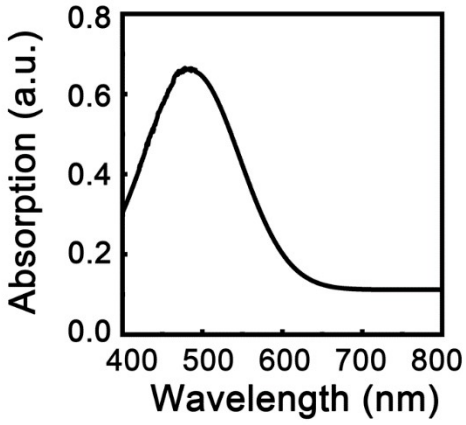

Fig. S4. The UV-Vis absorption spectra of CuSe nanoflakes.

5. Surface-enhanced Raman scattering (SERS) spectra of ABTS on flower-like CuSe under excitation at different wavelengths.

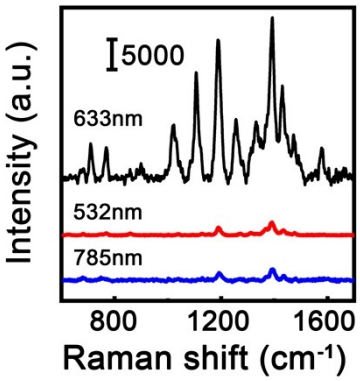

Fig. S5. SERS spectrum of 1 μM ABTS on flower-like CuSe under excitation at 633nm and 100 μM ABTS on flower-like CuSe under excitation at 532nm and 785nm.

6. Finite-difference time-domain (FDTD) calculations of flower-like CuSe under excitation at different wavelengths.

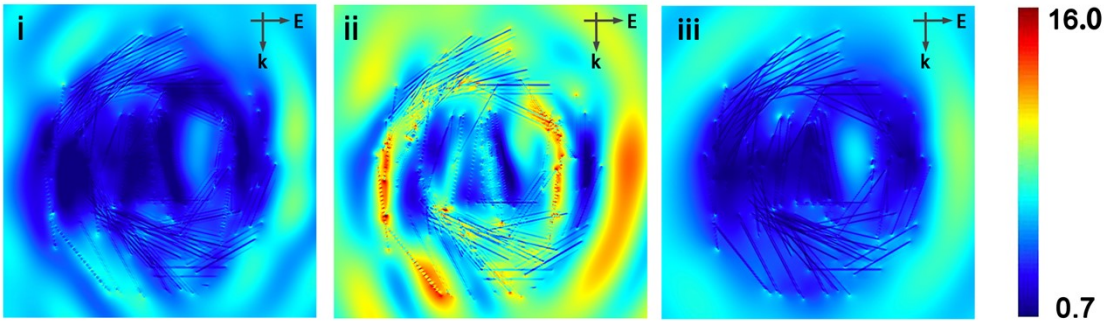

Fig. S6. Finite-difference time-domain (FDTD) calculations of flower-like CuSe under excitation at (i) 532 nm, (ii) 633nm and (iii) 785nm.

7. Transient absorption (TA) spectroscopic measurements of CuSe, CuSe-ABTS and CuSe-ABTS$^{\cdot+}$ under excitation at 633 nm laser.

The CT process between molecules and CuSe nanoflowers was then investigated through transient absorption (TA) spectroscopic measurements. Fig. S7 shows a transient absorption band of CuSe and CuSe-ABTS centered at 389 nm with the excitation of 633 nm laser, which assigned to excited electrons of CuSe. Due to the rapid charge recombination of the electrons and holes produced in CuSe, the electrons decayed in the short time range of 16.2 ps. Similarly, extensive electron absorption in CuSe-ABTS$^{\cdot+}$ was observed in the range of 389 nm to 520nm. However, in contrast to the lifetime of CuSe and CuSe-ABTS, the time profiles of the TA spectra at 389 nm for CuSe-ABTS$^{\cdot+}$ were fitted by two-exponential functions. The decay lifetime in CuSe-ABTS$^{\cdot+}$ was much shorter than that in CuSe and CuSe-ABTS, suggesting the efficient CT process. Thus, direct evidence for CT from CuSe to ABTS$^{\cdot+}$ was provided by TA results, and SERS activity of CuSe was much enhanced for ABTS$^{\cdot+}$.

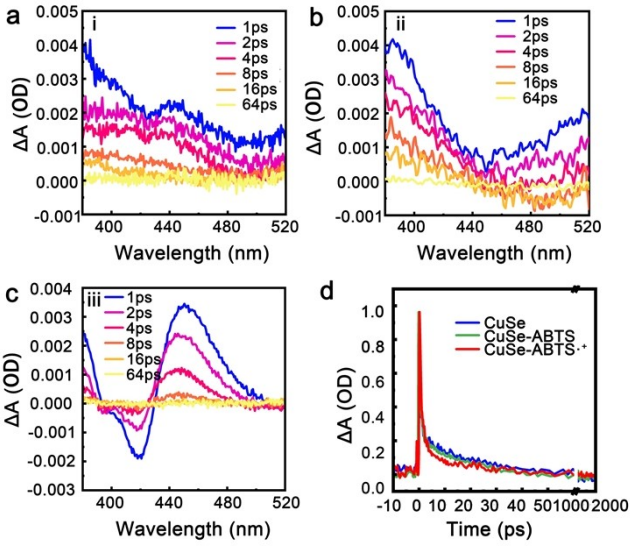

Fig. S7. Transient absorption (TA) spectroscopic measurements of (a) CuSe, (b) CuSe-ABTS and (c) CuSe-ABTS$^{\cdot+}$ after irradiation with a 633-nm laser excitation. (d) Time profiles of normalized transient absorption of CuSe, CuSe-ABTS and CuSe-ABTS$^{\cdot+}$ with the excitation of 633 nm laser. OD, optical density.

8. SEM image of flower-like CuSe immobilized on paper.

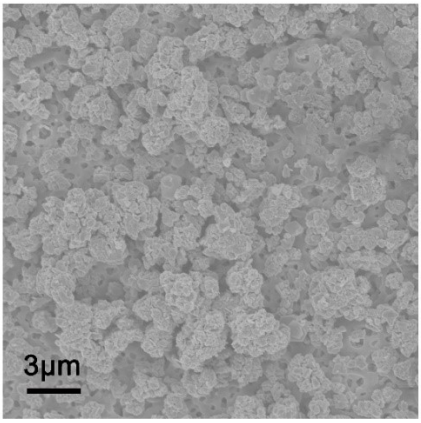

Fig. S8. SEM image of flower-like CuSe immobilized on paper.

9. UV−vis, photothermal and SERS responses in phosphate buffered saline and plasma.

We compared the response of our devices to miR-34c in buffer solution (PBS, pH=7.4) with plasma media. As shown in Fig. S9, little difference between buffer solution and plasma media was observed in UV-Vis absorption, temperature and Raman responses, indicating that the duplex structures were stable in complex plasma media, which ensured the good analytical activity of the device in plasma.

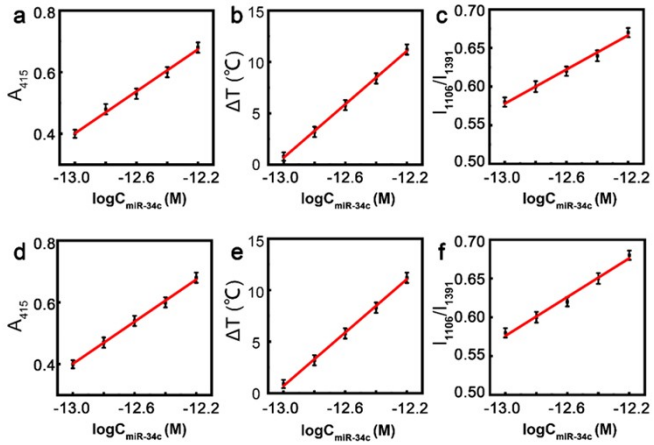

Fig. S9. (a) UV−vis, (b) photothermal and (c) SERS responses in buffer solution, (d) UV−vis, (e) photothermal and (f) SERS responses in plasma. Standard addition method was used for the determination.

10. Comparison of UV−vis, photothermal and SERS responses of DNA probes with and without extra base sequences in solid paper and buffer solution.

To avoid the steric hindrance from the solid paper and the nanoparticles, we added 12 cytosines at the 5' end of capture DNA and 12 adenines at the 3' end of detector DNA. The extra base sequences at the end of the DNA provided enough space for the hybridization reaction for the DNA to the target miRNA. As shown in Fig. S10, compared to the responses on DNA probes without extra base sequences, the presence of extra base sequences effectively avoided steric hindrance and produced a more distinct response signal. Then, we also compared the signals of DNA probes on solid paper with those in liquid phase buffer solution. Negligible differences of response signals were observed on solid paper versus in buffer solution, further indicating that the extra 12 base sequences we added at the end of DNA effectively avoided steric hindrance in solid paper.

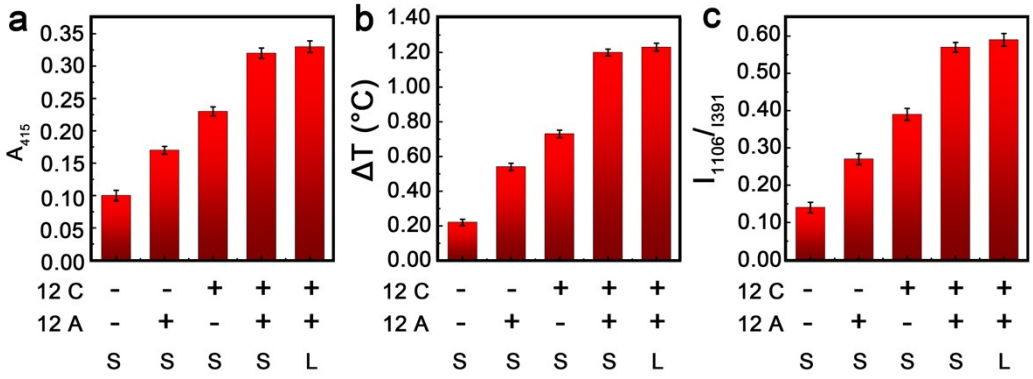

Fig. S10. Comparison of (a) UV−vis, (b) photothermal and (c) SERS responses with and without extra base sequences in solid paper and buffer solution. (12 C means the capture DNA with 12 cytosines at the 5' end; 12A means the detection DNA with 12 adenines at the 3' end; S means the measurements on solid paper; L means the measurements in liquid buffer solution; "+" means positive; "-" means negative).

11. Concentration optimization of various substances in the CuSe-catalyzed ABTS oxidization reaction system.

The concentration were optimized by exploring the effect of the concentrations of ABTS, CuSe and H_2O_2 on the tri-modal responses of diagnostic paper device toward miR-34c. When optimizing the concentration of each component, keep the concentration of other components and temperature unchanged, measure the UV-Vis, temperature and Raman response, and select the concentration with the highest response as the optimal concentration. As shown in Fig. S11, 2 mM for ABTS as a catalytic substrate, 2.5 M for H_2O_2 as an oxidizing agent, and 0.03 nM for CuSe as the catalytic unit were selected as the optimal conditions in the CuSe-catalyzed ABTS oxidization reaction system.

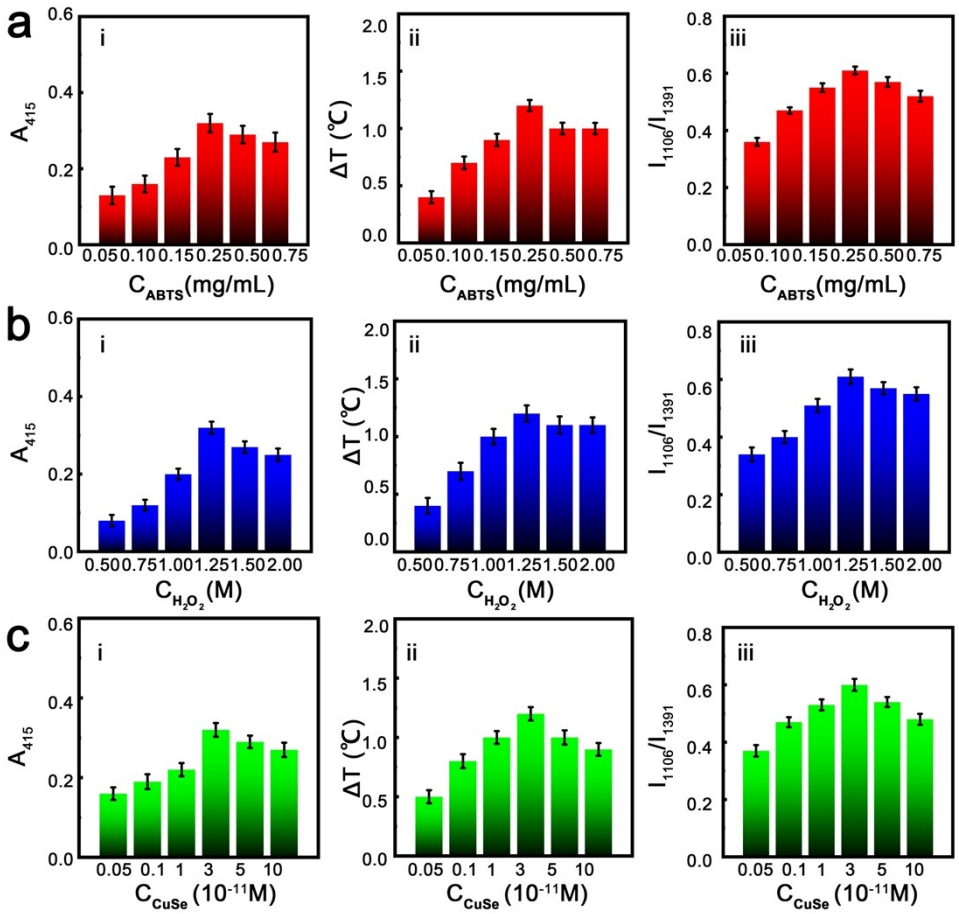

Fig. S11. Effect of the concentration of (a) ABTS, (b) H_2O_2 and (c) CuSe on the (i) A_{415}, (ii) temperature increase and (iii)I_{1106}/I_{1391}, respectively. Each data point represents the average value from seven results (S.D., n=7). Error bars equal to the standard deviations.

12. The feasibility of the CuSe-based tri-modal biosensing platform.

As shown in Fig. S12, samples (i-vi) with various substances in the CuSe-catalyzed ABTS oxidization reaction system, including the acetate buffer (0.1M, pH 4.2) as blank, (i) ABTS, (ii) ABTS+H_2O_2, (iii) CuSe, (iv) CuSe+ H_2O_2, (v) ABTS+CuSe, and (vi) CuSe+ABTS+ H_2O_2. UV-Vis spectra and colors in samples (i-v) did not change obviously, while obvious absorbances at around 415, 650, 730 and 825 nm appeared in sample (vi) with a clear green color (Fig. S12a and 12b). The result confirmed the peroxidase-mimicking properties of CuSe with characteristic absorption peaks of the oxidized product $ABTS^{\cdot+}$.[S1] On account of the strong photothermal conversion effect of $ABTS^{\cdot+}$ under 808 nm laser irradiation, a significant temperature elevation of ~15℃ was observed in sample (vi) (Fig. 12a). Remarkably, compared with samples (iii-iv), ABTS exhibited characteristic Raman peaks at 1391 cm^{-1} in samples (i-ii, v)(Fig. 12c), which was recognized as the phenyl ring breathing vibration (for details, see Table S3). After the ABTS was oxidized to $ABTS^{\cdot+}$ in the presence of both CuSe and H_2O_2 in sample (vi), Raman peak intensities at 1391 cm^{-1} were further elevated, which was ascribed to occurrence of the additional chemical enhancement of Raman signals of $ABTS^{\cdot+}$ on flower-like CuSe. Besides, a new peak at 1106 cm^{-1} appeared because the attraction of N atoms to the electron cloud of the adjacent C atoms of thiazole increased, resulting in the increase in polarizability of C-N bonds in thiazole moiety.[S2]

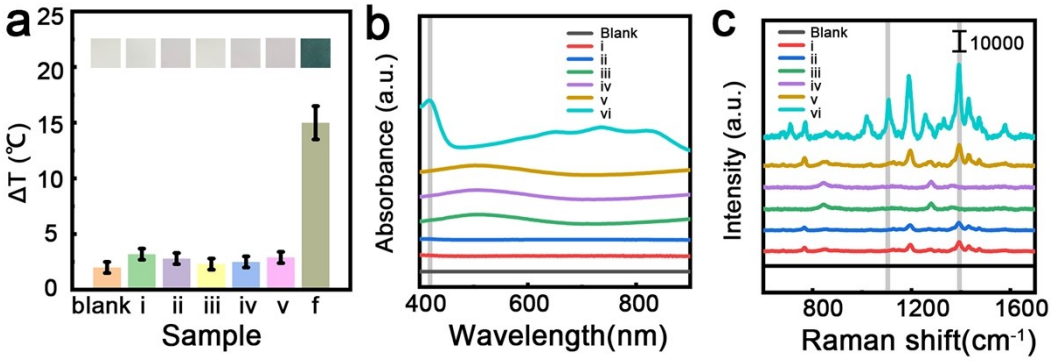

Fig. S12 (a) temperature increases (insets: photographs of detection unit), (b) UV−vis absorption spectra and (c) Raman spectra of different components in the CuSe-catalyzed ABTS oxidization reaction system, including the acetate buffer as blank, (i) ABTS, (ii) ABTS+H_2O_2, (iii) CuSe, (iv) CuSe+H_2O_2, (v) ABTS+CuSe, and (vi) CuSe+ABTS+H_2O_2.

13. Optimization of experimental parameters of the CuSe-based diagnostic paper device.

The molar ratio of capture DNA probe and detector DNA probe at 20:1 revealed the optimum absorption, photothermal and SERS performance. In addition, the peak intensity of absorption, photothermal and SERS reached the maximum at 37°C, while ascended with the pH value from 1 to 7 and then descended with the sequential increase of pH value. Thus, a molar ratio of 20:1, incubation temperature of 37°C and pH 7.0 were selected as the optimal conditions for miR-34c tri-modal analysis. Under these optimized conditions, reaction occurred instantly and complete within 15 min. Then, by passing different levels of water vapor into sealed bags containing dry air, we established test environments with different humidity levels. Our device exhibited stable signal output under different humidity conditions, indicating that ambient humidity had negligible effect on the measurements. Finally, we used a Xe lamp as the light source to simulate daylight exposure (AM 1.5G, intensity: 100 mW cm^{-2}) to test the effect of light conditions on the measurements. Compared to dark conditions, the color-temperature-Raman responses of devices remained stable under 5 days of daylight exposure, indicating that our device was not affected by light conditions.

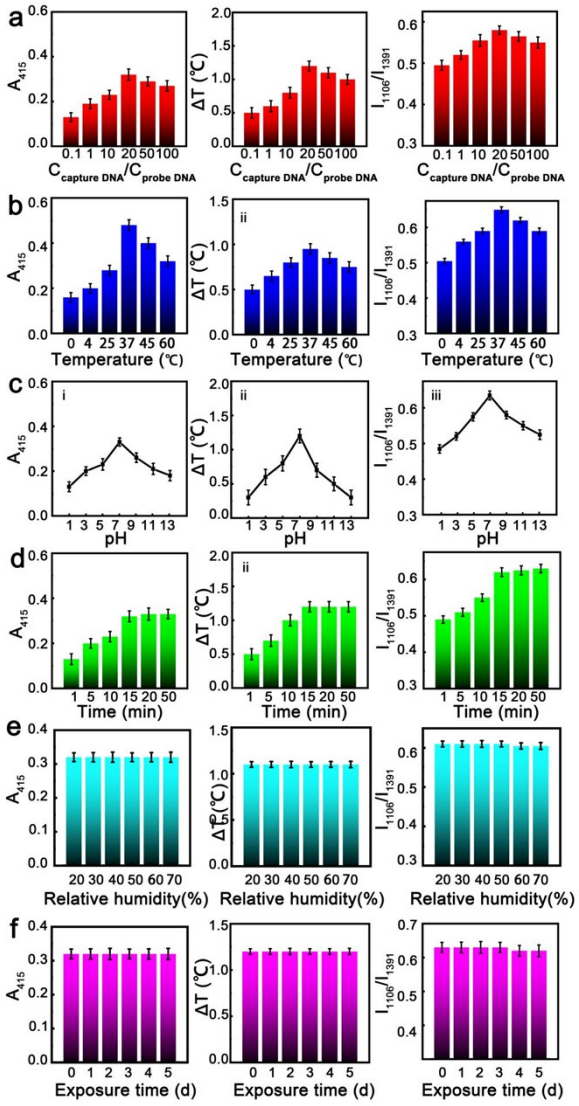

Fig. S13. Effect of (a) $C_{capture\ DNA}/C_{probe\ DNA}$, (b) incubation temperature, (c) pH, (d) detection time, (e) humidity and (f) exposure time under Xe lamp (AM 1.5G, intensity: 100 mW cm^{-2}) on the (i) A415, (ii) temperature increase and (iii)I1106/I1391, respectively. Each data point represents the average value from seven results (S.D., n=7). Error

bars equal to the standard deviations.

14. Selectivity tests of the CuSe-based diagnostic paper device.

The selectivity of the paper device was further evaluated by measuring its response in the presence of ions, amino acids, proteins and RNA sequences. As illustrated in Fig. S13, the addition of the interfering compounds in the absence of miR-34c showed an indiscernible colorimetric, absorption, temperature and SERS response, indicating the uniqueness of miR-34c for CuSe-based diagnostic paper device.

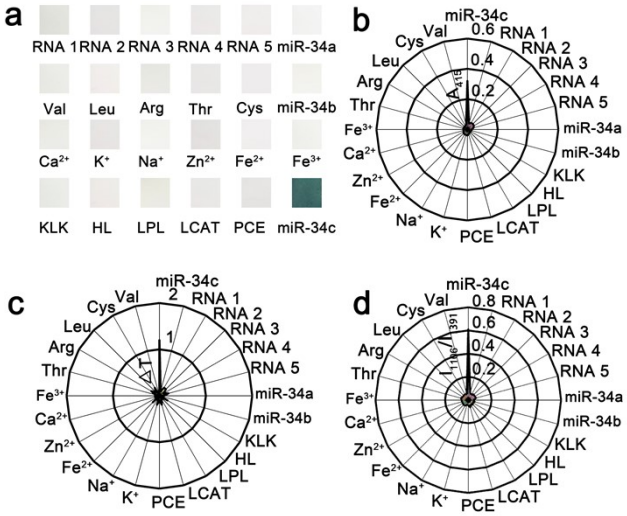

Fig. S14. Selectivity tests of (a) color, (b) UV−vis, (c) photothermal and (d) SERS mode of the paper device for miR-34c monitoring against ions, amino acids, proteins and RNA sequences. (KLK: kallikrein; HL: hepaticlipase; LPL: lipoprteinlipase; LCAT: acid phosphatase; PCE: pseudocholinesterase.)

15. Competition tests of the CuSe-based diagnostic paper device.

For the competition test, the effect of all these substances on the color-temperature-Raman response for miR-34c were investigated. Relatively little changes (< 4.7%) were observed. Especially, negligible changes (<3.2%) of I_{1106}/I_{1391} were observed upon the subsequent addition of these potential interferences after the

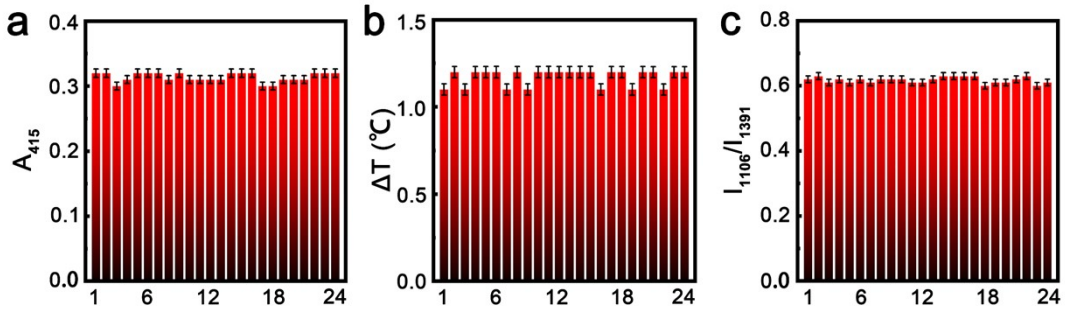

addition of miR-34c.

Fig. S15. Competition tests of (a) UV−vis, (b) photothermal and (c) SERS mode of the paper device for miR-34c monitoring against ions, amino acids, proteins and mismatched RNA sequences. (1-21: miR-34c, K+, Na^+, Fe^{2+}, Fe^{3+}, Zn^{2+}, Ca^{2+}, Thr, Arg, Leu, Cys, Val, KLK, HL, LPL, LCAT, PCE, RNA 1, RNA 2, RNA 3, RNA 4, RNA 5, miR-34a, miR-34b) (KLK: kallikrein; HL: hepaticlipase; LPL: lipoprteinlipase; LCAT: acid phosphatase; PCE: pseudocholinesterase.) (n=5, S. D.).

16. Stability of the CuSe-based diagnostic paper device.

The temperature, UV-Vis absorption and Raman spectra of CuSe-based diagnostic paper device within a 6-month period were collected. 10 μL PBS solution containing 110 fM miR-34c was added to the device and measured for 7 times each month.

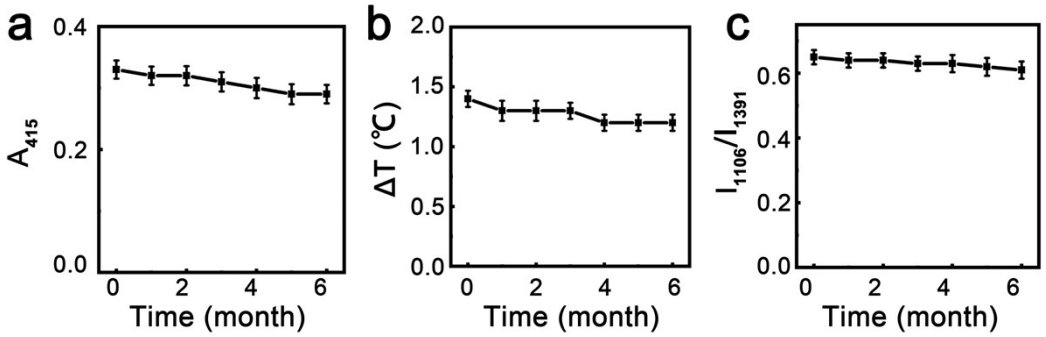

Fig. S16. Evaluation of the stability of the device by using (a) UV−vis, (b) photothermal and (c) SERS mode.

17. Repeatability of the CuSe-based diagnostic paper device.

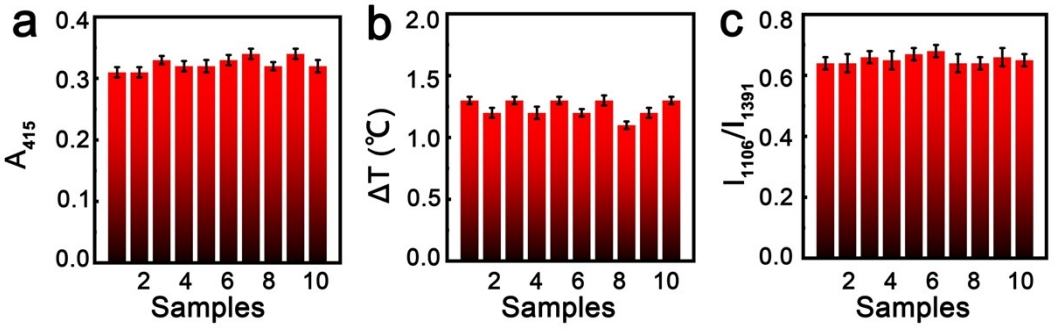

Fig. S17. Evaluation of the repeatability of the device by using (a) UV−vis, (b) photothermal and (c) SERS mode.

18. Absorption, temperature and Raman analysis of miR-34c in whole blood.

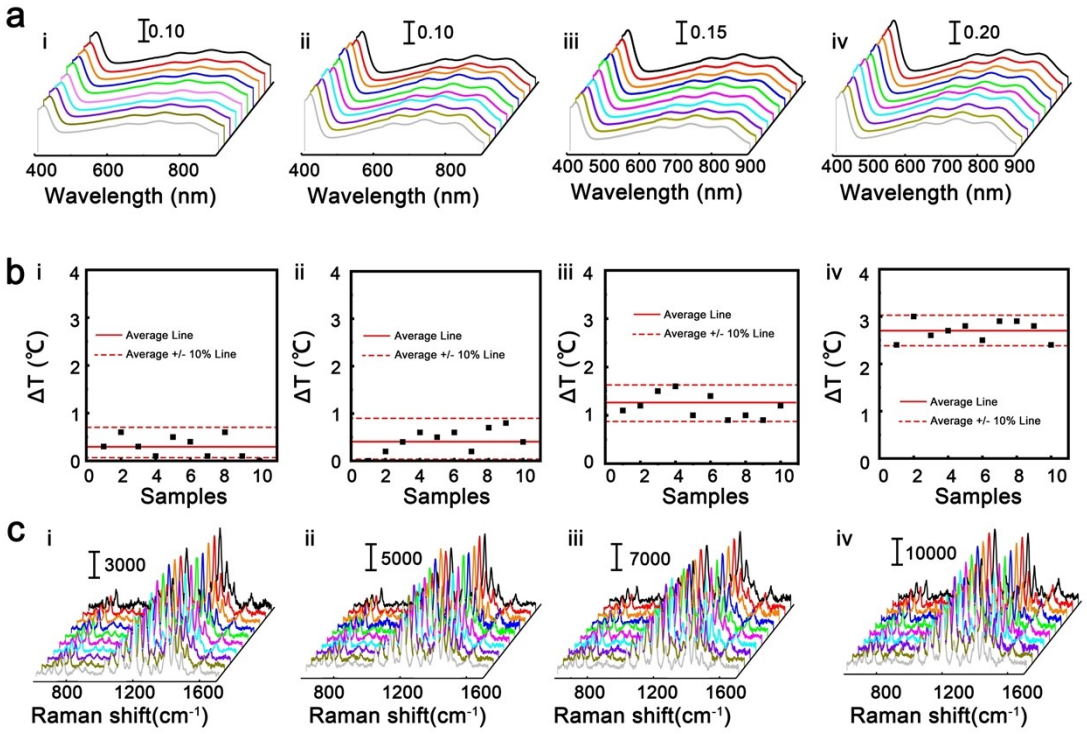

Fig. S18. (a) Absorption, (b) temperature and (c) Raman analysis of miR-34c in whole blood of (i) control normal mice, (ii) early-stage AD mice, (iii) middle-stage AD mice and (iv) late-stage AD mice, respectively.

19. Calculation of the bandgap energy (Eg) for flower-like CuSe.

The inset of Fig. 1c shows the reflectance spectrum of flower-like CuSe transformed according to Eq 1 plotted against the photon energy. The x-axis intersection point of the linear fit of the Tauc plot gives an estimate of the band gap energy. Thus, the estimated band gap for the flower-like CuSe were about 1.83 eV.

$$\text{Eq 1: } (\alpha \cdot v)^{1/\gamma} = B(hv - Eg)$$

20. Enhancement factor calculations for ABTS and ABTS$^{\cdot+}$ on flower-like CuSe.

Table S1. Comparison of enhancement factor of flower-like CuSes for ABTS and ABTS$^{\cdot+}$

Molecules on flower-like CuSe	ABTS	ABTS$^{\cdot+}$
EF value	1.58×10^{6}	2.14×10^{7}

The calculation methods.

Enhancement factor (EF) for each nanomaterial was calculated by Eq 2.

$$\text{Eq 2: } EF = (I_{SERS} / N_{SERS}) / (I_{bulk} / N_{bulk})$$

I_{SERS} and I_{bulk} are the intensities of the selected Raman peak in the SERS and non-SERS spectra, and N_{SERS} and N_{bulk} are the average number of molecules in scattering area for SERS and non-SERS measurement.

For ABTS, N_{SERS} and N_{bulk} can be estimated as:

$$N_{bulk} = 100\ \mu L \times 10^{-3}\ mol / L \times 6.02 \times 10^{23}\ mol^{-1} \times 2.92\ \mu m^2 / 0.16\ cm^2$$

$$N_{SERS} = 10\ \mu L \times 10^{-7}\ mol / L \times 6.02 \times 10^{23}\ mol^{-1} \times 2.92\ \mu m^2 / 0.16\ cm^2$$

where d is the diameter of the light spot d = 1.22 λ/NA, λ is incident wavelength 633 nm, the numerical

aperture of the objective lens N_A = 0.4, thereby, Laser spot size (π (d/2)^2) is about 2.92 μm^2. I_{SERS} and I_{bulk} were obtained on the peak intensity at 1391 cm^{-1} in the SERS and non-SERS spectra, I_{SERS}=3160 and I_{bulk}=200. The EF could be calculated to be around 1.58×10^6.

For ABTS$^{\cdot}$, N_{SERS} and N_{bulk} can be estimated as:

$$N_{bulk} = 200\ \mu L \times 10^{-3}\ mol / L \times 6.02 \times 10^{23}\ mol^{-1} \times 2.92\ \mu m^2 / 0.16\ cm^2$$

$$N_{SERS} = 10\ \mu L \times 10^{-7}\ mol / L \times 6.02 \times 10^{23}\ mol^{-1} \times 2.92\ \mu m^2 / 0.16\ cm^2$$

I_{SERS}=220 and I_{bulk}=23630, and the EF value was calculated to be 2.14×10^7.

21. Calculation of valence band (VB) and conduction band (CB) of flower-like CuSe.

$$\text{Eq 3: } EN = \frac{EA + IE}{2}$$

$$\text{Eq 4: } EN(X_nY_m) = \sqrt[n+m]{EN(X)^n E (N)^m}$$

$$EN(CuSe) = \sqrt[1+1]{4 \cdot \times 45\ 8\ \&} = 5.14$$

$$EA = EN - \frac{E_g}{2} = 5.14 - \frac{1.83}{2} = 4.22\ eV$$

$$IE = EN + \frac{E_g}{2} = 5.14 + \frac{1.83}{2} = 6.05\ eV$$

22. Calculation of Gibbs free energy.

The stability of the DNA-RNA duplex structure is determined by the stability of the base pairs of DNA-RNA, which can be expressed in terms of Gibbs free energy (ΔG). According to the method proposed by Breslauer et al.[S2], the ΔG of a base pair is the sum of the ΔG of adjacent base on DNA strands. The ΔG between different base pairs are tabulated in Table S2.

Table S2. Gibbs free energy between different base pairs.

Post-base / Pre-Base	dA	dC	dG	dT
dA	-1.9 kcal/mol	-1.3 kcal/mol	-1.6 kcal/mol	-1.5 kcal/mol
dC	-1.9 kcal/mol	-3.1 kcal/mol	-3.6 kcal/mol	-1.6 kcal/mol
dG	-1.6 kcal/mol	-3.1 kcal/mol	-3.1 kcal/mol	-1.3 kcal/mol
dT	-1.0 kcal/mol	-1.6 kcal/mol	-1.9 kcal/mol	-1.9 kcal/mol

Thus, the ΔG of capture DNA-miR-34c duplex and Detector DNA-miR-34c were calculated through Eq 5 and Eq 6 as follow:

Eq5: ΔG (Capture DNA -miR34c) = ΔG (GCAATC) = ΔG (GC)+ ΔG (CA)+ΔG (AA)+ ΔG (AT)+ ΔG (TC)=-3.1-1.9-1.9-1.5-1.6=-10 kcal/mol

Eq6: ΔG (Detector DNA- miR34c) = ΔG (AGCTAACTACACTGCCT)= ΔG (AG)+ΔG (GC) +ΔG (CT)+ΔG (TA)+ΔG (AA)+ΔG (AC)+ΔG (CT)+ΔG (TA)+ΔG (AC)+ΔG (CA)+ΔG (AC)+ΔG (CT) +ΔG (TG)+ΔG (GC)+ΔG (CC)+ΔG (CT)=-1.6-3.1-1.6-1.0-1.9-1.3-1.6-1.0-1.3-1.9-1.3-1.6-1.9-3.1-3.1-1.6=-28.9 kcal/mol

Both the ΔG values were negative, which revealed that the DNA-RNA hybridization in the work was a spontaneous process thermodynamically, indicating the great thermodynamic stability of two structures[S3].

23. Peak assignments of SERS spectrum of ABTS and ABTS·+.

Table S3. Peak assignments of SERS spectrum of ABTS and ABTS·+ [S4]

Raman shift (cm^{-1})	Vibrational Modes
1018	C-N stretching vibration
1106	C-N out-of-plane bending
1194	C-H rocking vibration
1391	phenyl ring breathing vibration
1434	C-H out-of-plane bending vibration
1473	C-H out-of-plane bending vibration

24. The limit of detection (LOD) calculations of SERS, UV-Vis and photothermal methods.

The standard curve is given as Eq 5, where A and B are the variable obtained via least-square root linear regression for the signalconcentration curve and variable Y represents the normalized signal at miR-34c concentration of C. SD is the standard deviation and Y_{blank} is the signal of the blank sample. The LOD is calculated as Eq 8.

$$\text{Eq 5: } Y = A + B \times \log C$$

$$\text{Eq 6: } SD = \sqrt{\frac{1}{n-1} \times \sum_{n}^{i} (X_i - X_{average})^2}$$

$$\text{Eq 7: } LOD = 10^{[(Y_{blank} + 3SD) - A]/B}$$

For the photothermal method, Y represents the normalized temperature increases, and the linear regression was: Y =176.246+13.52 × logC. A=176.2, B=13.5, Y_{blank} = 0.1, SD = 0.06.

$$LOD = 10^{[(Y_{blank} + 3SD) - A]/B} = 10^{[(0.1 + 3 \times 0.06) - 176.2]/13.5} = 10^{-13.03} = 9.3 \times 10^{-14}\ (M)$$

For the UV-Vis method, Y represents the normalized UV-Vis absorption signals at 415nm, and the linear regression was: Y =7.46+0.55 × logC. A=7.46, B=0.55, Y_{blank} = 0.11, SD = 0.05.

$$LOD = 10^{[(Y_{blank} + 3SD) - A]/B} = 10^{[(0.11 + 3 \times 0.05) - 7.46]/0.55} = 10^{-13.1} = 7.9 \times 10^{-14}\ (M)$$

For the photothermal method, Y represents the normalized ratiometric SERS signal (I_{1106} / I_{1391}), and the linear regression was: Y =1.95+0.11 × logC. A=1.95, B=0.11, Y_{blank} = 0.15, SD = 0.03.

$$LOD = 10^{[(Y_{blank} + 3SD) - A]/B} = 10^{[(0.15 + 3 \times 0.03) - 1.95]/0.11} = 10^{-15.3} = 5.0 \times 10^{-16}\ (M)$$

25. Comparison of miR-34c concentrations in whole blood at different stages of AD using CuSe-based diagnostic paper device and RT-PCR.

Table S4. Comparison of miR-34c concentrations in whole blood at different stages of AD using CuSe-based

diagnostic paper device and RT-PCR.

	UV-Vis Spectra		Temperature		Raman Spectra		RT-PCR	
	Average	RSD	Average	RSD	Average	RSD	Average	RSD
NC	/	/	/	/	32±3 fM	3.8%	32±6 fM	7.6%
Early stage	/	/	/	/	63±5 fM	3.8%	63±8 fM	7.9%
Middle stage	111±8 fM	4.3%	110±9 fM	7.2%	110±5 fM	1.7%	110±13 fM	9.5%
Late stage	153±9 fM	3.6%	155±8 fM	6.1%	154±4 fM	1.1%	154±11 fM	8.8%

References

[S1] W. Yang, X. Shi, Y. Shi, D. Yao, S. Chen, X. Zhou and B. Zhang, *ACS Nano*, 2018, **12**, 12169-12180.

[S2] J. Liu, Z. Liu, W. Wang and Y. Tian, *Angew. Chem. Int. Ed.*, 2021, **60**, 2-11.

[S3] K. J. Breslauer in *Thermodynamic Data for Biochemistry and Biotechnology*. ed. H. J. Hinz Springer, Berlin, Heidelberg, 1st, 1986, Chapter 15, 402–427.

[S4] A. Garcia-Leis, D. Jancura, M. Antalik, J. V. Garcia-amos, S. Sanchez-Cortesa and Z. Jurasekova, *Phys. Chem. Chem. Phys.*, 2016, 18, 26562-26571.